metals

MDPI

Article

Peculiarities of the Creep Behavior of 15Kh2NMFAA Vessel Steel at High Temperatures

Egor Terentyev, Artem Marchenkov *, Vladimir Loktionov, Anastasia Pankina, Georgy Sviridov, Ksenia Borodavkina, Danila Chuprin and Nikita Lavrik

National Research University Moscow Power Engineering Institute, 14/1, Krasnokazarmennaya Street, 111250 Moscow, Russia; terentyevyv@mpei.ru (E.T.); loktionovvd@mpei.ru (V.L.); pankinaaa@mpei.ru (A.P.); sviridovgeorb@mpei.ru (G.S.); borodavkinaxt@mpei.ru (K.B.); chuprindv@mpei.ru (D.C.); lavriknv@mpei.ru (N.L.)

* Correspondence: art-marchenkov@yandex.ru

Abstract: The creep properties of 15Kh2NMFAA nuclear WWER (water–water energetic reactor) vessel steel in the range of 500–1200 °C temperatures, which may appear during severe nuclear reactor accidents, were investigated. The present paper attempts to analyze the creep curves obtained from tensile testing at high temperatures using the Larson–Miller parametric technique. The power law rate and material coefficient of Norton's equation with the Monkman–Grant relationship coefficient were found for each test temperature. It is shown that in accordance with the Monkman–Grant relationship coefficient values, changing the creep type from dislocation glide to high temperature dislocation climb occurs in the temperature range of 600–700 °C, which leads to a slope change in the Larson–Miller parameter plot and the conversion of steel creep behavior. It is also shown that in the range of A_1–A_3 temperatures, a stepwise change in creep characteristics occurs, which is associated with phase transformations. In addition, the constancy of the product of the time to rupture τ_r and the minimum creep rate $\dot{\epsilon}_{min}$ in the ranges of 600–700 °C and A_3—1200 °C was noted. The proposed approach improves the accuracy of time to rupture estimation of 15Kh2NMFAA steel by at least one order of magnitude. Based on the research results, the calculated dependence of the steel's long-term strength limit on temperature was obtained for several time bases, allowing us to increase the accuracy of material survivability prediction in the case of a severe accident at a nuclear reactor.

Keywords: 15Kh2NMFAA steel; creep; microstructure; Larson–Miller parameter; Monkman–Grant relationship; long-term strength limit

Academic Editors: Elisabetta Gariboldi and Jiapo Wang

Received: 20 April 2025
Revised: 20 May 2025
Accepted: 21 May 2025
Published: 22 May 2025

Citation: Terentyev, E.; Marchenkov, A.; Loktionov, V.; Pankina, A.; Sviridov, G.; Borodavkina, K.; Chuprin, D.; Lavrik, N. Peculiarities of the Creep Behavior of 15Kh2NMFAA Vessel Steel at High Temperatures. *Metals* **2025**, *15*, 571. https://doi.org/10.3390/met15060571

1. Introduction

One of the key problems in the analysis of reactor behavior during a severe accident at a nuclear power plant (NPP) is the problem of the in-vessel retention (IVR) measure of destroyed core materials during the emergency. The IVR strategy was first designed [1] for the Finnish Loviisa NPP for the WWER-440 reactor unit and was further successfully implemented in NPPs operating AP-600 and AP-1000 nuclear reactors [2,3].

A review of studies [1–11] analyzing the behavior of reactor vessels under conditions of intense thermal and force impact in an accident with complete or partial core destruction has shown that the main cause of reactor vessel structural failure is the high-temperature creep of the vessel material. Therefore, an adequate assessment of the reactor vessel's ability to resist deformation under creep conditions, as well as the prediction of the rupture time

in such severe accidents, is an extremely crucial task and is the subject of comprehensive studies [12–17].

Heat-resistant 15Kh2NMFAA steel is one of the most commonly used steels for WWER nuclear vessel manufacture [18,19]. The requirements for the chemical composition of this steel and actual composition of the steel used in this research is shown in Table 1.

Table 1. Content of elements in 15Kh2NMFAA steel, wt. % (Req.—requirements of the standard; Act.—actual content in the steel under study).

	C	Mn	Si	Cr	Ni	Mo	V	P	S
Req.	0.13–0.18	0.30–0.60	0.17–0.37	1.80–2.30	1.00–1.50	0.50–0.70	0.10–0.12	≤0.012	≤0.015
Act.	0.15	0.6	0.32	2.09	1.2	0.57	0.1	0.009	0.002

This steel was developed in the USSR over 60 years ago for the manufacture of WWER reactor vessels and other power equipment elements. Over time, the steel has undergone numerous changes in chemical composition, as well as manufacturing and processing technologies, to meet the requirements for such materials and ensure the reliable operation of reactor vessels for at least 30 years. The experience of operating vessels made of this steel in Russia and other countries has shown its fairly high reliability. The service life of most reactor vessels is extended today to 40, 50, and even 60 years. At the same time, such service life is possible only at nominal temperatures, which are about 300 °C. The behavior of this steel at a significant increase in temperature up to 500 °C and above, which can only be observed in the case of severe accidents at a NPP, deserving special attention.

Numerical studies are dedicated to the investigation of creep behavior, microstructure changes, and factors affecting the strain and damage accumulation of various heat-resistant steels and alloys at high temperatures [20–34]. Several results of creep tensile tests in the range of 500–1200 °C of 15Kh2NMFAA steel were presented in previous authors' papers [35–37], where some specific deviations in the steel creep strain at temperatures between 600° and 850 °C were observed. The explanation assumed to be due to microstructure changes in the range of A_1–A_3 phase transition temperatures ($A_1 \approx$ 760–770 °C is the temperature of pearlite to austenite conversion and $A_3 \approx$ 820–830 °C is the temperature of ferrite to austenite conversion finish during heating). It was shown that the results of predicted rupture time for 700 °C obtained using the Larson–Miller equation for temperatures between 500 °C and 900 °C without taking into consideration the microstructure changes of the 15Kh2NMFAA steel differs from ones obtained by creep tensile testing more than 20 times [35]. Thus, for an applied stress of 35 MPa at a temperature of 750 °C, the estimated failure time is 3410 h, whereas during creep testing, the specimens were failed in 20–21 h. There are several papers that study the microstructure impact on the creep characteristics of reactor steels, for example, SA508 steel [16]. However, the A_1 temperature for SA508 steel is much lower, so for this steel, the transition to hot deformation coincides with the onset of phase transformations. The behavior of 15Kh2NMFAA steel, which contains a larger number of ferritizing elements and has significantly higher A_1 and A_3 temperatures is different. It is obvious that the creep behavior has not been studied in enough detail for this steel yet.

The present paper attempts to define the creep behavior of the 15Kh2NMFAA steel in the range of 500–1200 °C, in connection with phase transformations and microstructure changes that are taking place under variable loading and temperature. The main task of the paper is obtaining and analyzing real data on the creep behavior of 15Kh2NMFAA steel at temperatures corresponding to abnormal operating conditions of the reactor vessel which may occur in case of severe accidents. These data are of great value for assessing the reliability of power engineering equipment at nuclear power plants.

2. Materials and Methods

Cylindrical specimens with a diameter of ∅8 mm for creep tension tests were machined off from an actual unreserved WWER pressure vessel. Creep tests were carried out on tensile machines at temperatures of 500–1200 °C. The 1246R-2/2300 testing machines, NIKIMT, Moscow, Russia were used for specimen testing, which are designed to perform creep tests, including tests in a vacuum, up to a temperature of 2300 °C. The machines have an electromechanical drive. The load is measured by a strain gauge, and the strain is measured by a strain gauge extensometer. Both sensors are located inside the vacuum chamber and allow recording the creep curves "load—time" and "strain—time". The stress level varied depending on the test temperature. At temperatures up to 650 °C, tests were carried out in an air atmosphere, at temperatures of 700–900 °C in argon, and at temperatures of 900–1200 °C in a vacuum. In total, more than 60 specimens were tested, and 56 specimen test results were accepted for consideration and analyzed. All specimens test results are shown in Table A1 (see Appendix A at the end of the paper).

For the creep curve analysis and experimental data processing, the following parameters were used: stress σ, temperature T, rupture time τ_r, and minimum creep rate $\dot{\epsilon}_{min}$. A Larson–Miller parametric technique was used for obtaining relations between stress, temperature, and rupture time for experimental data as follows:

$$\log \sigma = b_1 + b_2 P_{LM}, \quad (1)$$

$$P_{LM} = T(\log \tau_r + C), \quad (2)$$

where P_{LM} is the Larson–Miller parameter, and b_1, b_2, and C are the fitting constants. The Larson–Miller constant C, as mentioned in [23,24], can be varied with the materials and testing conditions ranging from 10 to 30. In [23], the Larson–Miller constant was determined to be C = 20 for carbon steels and low-alloy steels, which had a similar composition with that of SA508 Gr.3 steel. Therefore, the value of C = 20 was chosen in this paper.

The creep equation expressing the dependence of minimum creep rate $\dot{\epsilon}_{min}$ on stress σ at different constant temperatures was used as follows:

$$\dot{\epsilon}_{min} = Ae^{-Q/RT}\sigma^n, \quad (3)$$

where A and B are constants, Q is the activation energy, R is the gas constant, and n is the creep stress exponent. One of the most important creep parameters for engineering applications is rupture time τ_r. For heat-resistant low-alloyed steels, τ_r is inversely related to the creep rate at the steady state (minimum creep rate $\dot{\epsilon}_{min}$) according to the Monkman–Grant relationship, expressed as follows:

$$\tau_r = K/\dot{\epsilon}_{min}, \quad (4)$$

where K is a constant. The values of b_1, b_2, C, B, and K, used in Equations (1)–(4), were determined via data processing to maximize the coefficient of determination r^2.

To study the microstructure, the 15Kh2NMFAA steel specimens were axially cut after being tested. These fragments were pressed into a phenolic compound, consistently grinded using emery paper of different grits, and mechanically polished with colloidal suspension based on Al_2O_3. Microstructure analysis was performed using a Tescan MIRA 3 LMU scanning electron microscope, Tescan, Libušina, Czech Republic equipped with the high brightness Schottky Field Emission gun and Energy-dispersive X-ray spectroscopy (EDX) detector, Tescan, Libušina, Czech Republic.

3. Results

Experimental conditions and creep test results of the 15Kh2NMFAA steel specimens are presented in Table A1, and Figure 1 shows several creep curves for various test stresses and temperatures.

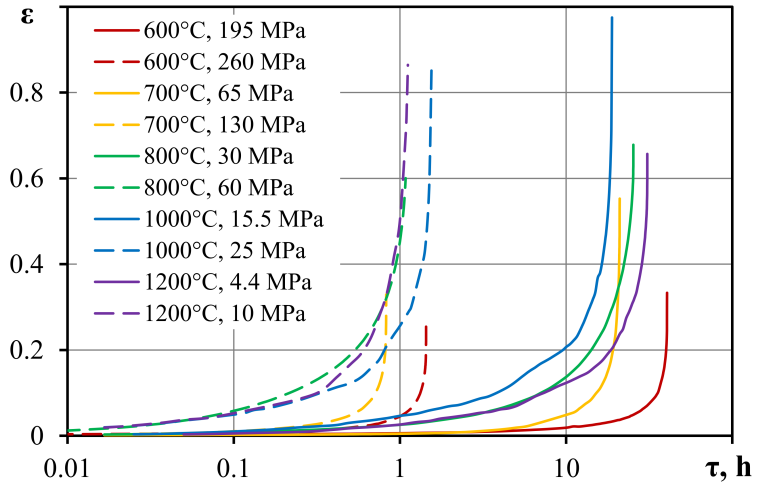

Figure 1. Creep curves "strain ϵ–time τ" of several 15Kh2NMFAA steel specimens.

A plot of stress σ vs. the Larson–Miller parameter P_{LM} for all tested specimens is shown in Figure 2, taking a value of $C = 20$. A perceptible slope change in the "$\sigma - P_{LM}$" relation in the range of 700–750 °C occurs, which could not be related to the steel microstructure type change, because the starting phase transition temperature A_1 is noticeably higher ($A_1 \approx$ 760–770 °C) for this steel [38]. Moreover, for the temperatures below 750 °C, at 800 °C and above 850 °C, a break and a shift in the trend line in Figure 2 are observed as the test temperature increases. The most plausible cause of this phenomenon is the changes in the microstructure that are taking place in the region of A_1 and A_3 temperatures.

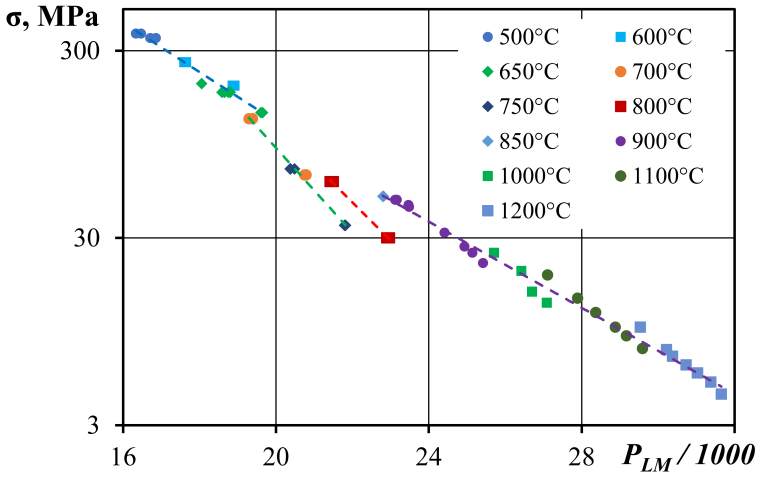

Figure 2. Plot of Larson–Miller Parameter P_{LM} for 15Kh2NMFAA steel at temperatures of 500–1200 °C.

Analyzing these results, the creep stress exponent n and parameter B values were calculated for each test temperature specified in Equation (3). Figure 3 shows the n and log$B$ values for different test temperatures. The graph indicates that the steepest drop in the power law exponent (3) occurs in the range of 600–700 °C, while in the range of 750–1200 °C, its value remains constant despite the phase transformations in the A_1–A_3 range.

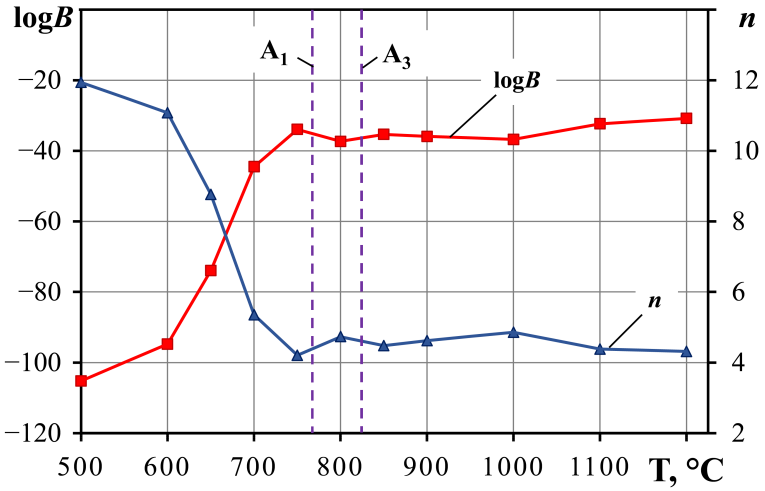

Figure 3. Relationship between the B and n coefficients of power law relation $\dot{\epsilon}_{min} = B\sigma^n$ and test temperature T.

Figure 4 shows the dependence of the coefficient K of the Monkman–Grant ratio, calculated for each test on the value of the rupture time τ_r multiplied by the minimum creep rate $\dot{\epsilon}_{min}$ using Equation (4). It follows from the results that in the ranges of 600–700 °C and A_3—1200 °C, coefficient $K = \tau_r\dot{\epsilon}_{min}$ remains constant, and the increase in the value of K occurs at 750 °C, that is, before the beginning of phase transformations at A_1 temperature.

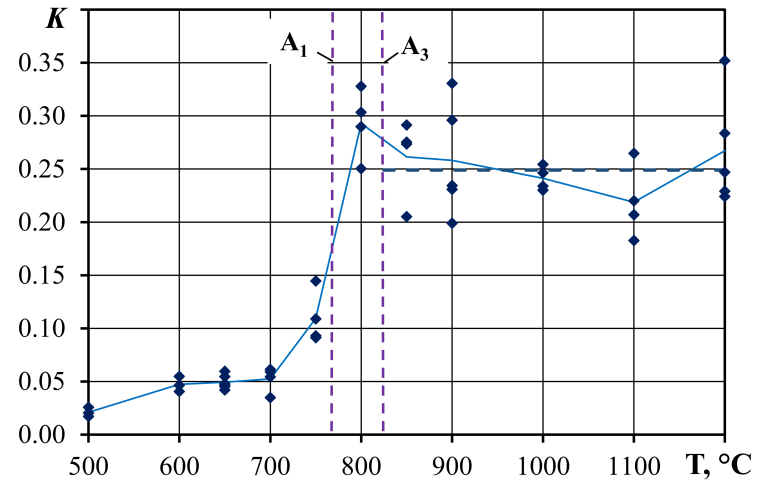

Figure 4. Dependence of the coefficient K of the Monkman–Grant ratio on test temperature T.

It is obvious from the obtained graphs that the microstructure has a decisive impact on the steel behavior under creep conditions. The original microstructure of the steel is represented by a ferrite–carbide mixture obtained after normalization and subsequent high tempering. Some results of 15Kh2MFAA steel microstructure investigation are presented in [38]. Dispersed particles, primarily carbides, play an important role in resistance to deformation under creep conditions. The distribution of carbide inclusions was studied by scanning electron microscopy (Figure 5).

Three types of carbides were found in the specimens tested at 800 °C and below as follows: molybdenum-enriched (light) with an average size of 100–300 nm, located for the most part at grain boundaries; chromium-enriched (gray) with an average size of 100–200 nm; and vanadium-enriched (dark) with an average size of 100 nm or less. According to [39], vanadium-enriched carbides are compounds of the Me(C,N) type, molybdenum-enriched ones are Me_2C, and chromium-enriched ones are Me_7C_3. No carbides were de-

tected in the specimen tested at 850 °C for 25.6 h. Apparently, this duration was sufficient to dissolve them. The size of vanadium-enriched carbides found in the specimen tested at 650 °C was smaller, and the volume fraction of carbides was less in comparison with the specimens tested at 800 °C and 850 °C.

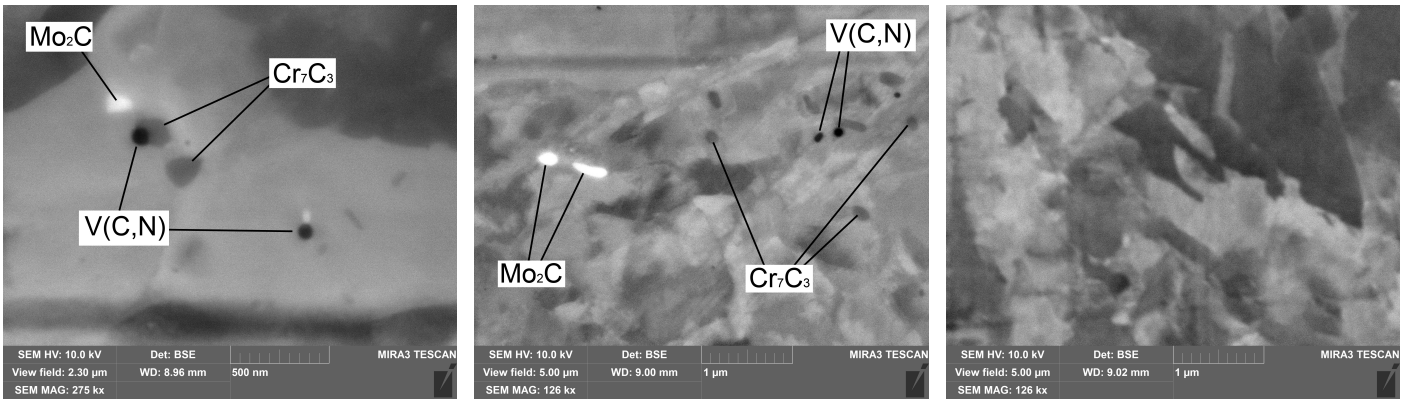

(**a**) (**b**) (**c**)

Figure 5. Microstructure of 15Kh2NMFAA steel after creep tests at 650 °C (**a**), 800 °C (**b**), and 850 °C (**c**).

4. Discussion

The creep curves of 15Kh2NMFAA do not have a clearly defined steady state region area, which was also noted during the long-term tests of similar steels [20,27]. Low-alloyed steels with a ferrite–carbide microstructure have relatively high yield strength due to precipitation and dislocation hardening and therefore do not usually require significant strain hardening to resist creep well. In this case, the primary stage of creep passes quickly into the secondary (steady state) stage, with a minimum of the strain rate $\dot{\epsilon}_{min}$, followed immediately by the tertiary stage with an abrupt increase in the strain rate.

The gap in the Larson–Miller parametric dependence for the temperatures of A_1 and A_3 (760–770 °C and 820–830 °C, respectively, as shown in Figure 2), indicates that 15Kh2NMFAA steel should be considered as different material when analyzing creep characteristics in the austenite and ferrite–carbide states due to fact that the lattice type and physical properties differ between these two microstructures. To accurately predict the creep behavior of 15Kh2NMFAA steel, it is reasonable to obtain the analytical stress dependences on the Larson–Miller parameter for various temperature ranges as follows: from 500 °C to 700 °C, from 700 °C to A_1, and from A_3 to 1200 °C. For the $A_1 - A_3$ temperature range, including tests at 800 °C, it is not reasonable to obtain the common "σ—P_{LM}" relation due to the continuous microstructure changes within this temperature range. Figure 6 "σ—P_{LM}" dependence for the specified temperature ranges. When constructing Figure 6, data from the same creep tests were used as for constructing the generalized Larson–Miller dependence shown in Figure 2.

To obtain the closest approximation functions, the coefficients b_1, b_2, and C were chosen independently for each temperature range. Table 2 shows the values of these coefficients for each temperature range, along with the maximum difference between the experimental and calculated stress ($\sigma^{exp}/\sigma^{calc}$) and rupture time ($\tau_r^{exp}/\tau_r^{calc}$) obtained from the Larson–Miller parametric relation (calculated values) and from creep test experiment data (experimental values). Thus, the estimated rupture time from this paper agrees well with the experimental data, with a worst-case difference of 1.83 times (Table 2), which is a much more accurate results than that obtained in previous research [35].

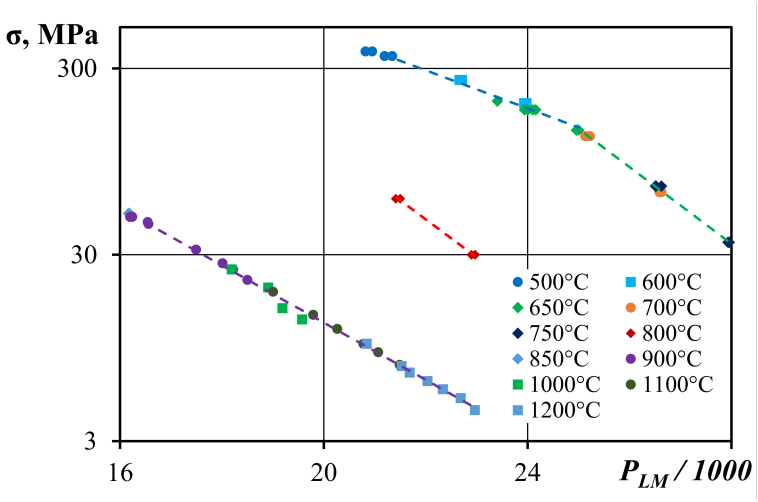

Figure 6. Stress σ—Larson–Miller parameter P_{LM} curves for 15Kh2NMFAA steel at different temperature ranges.

Table 2. Larson–Miller parameter b_1, b_2, and C coefficients for 15Kh2NMFAA steel at different temperature ranges.

T, °C	Larson–Miller Parameter Coefficients			Difference of Experimental and Calculated Values	
	b_1	b_2	C	$\sigma^{exp}/\sigma^{calc}$, MPa	$\tau_r^{exp}/\tau_r^{calc}$, h
500–650	4.71440	−0.10217	25.8	195.0/184.0	13.55/23.70
650–760	7.28976	−0.20549	26.0	70.0/65.9	1.06/0.80
800	6.13906	−0.20328	20.0	30.0/32.1	21.84/29.78
830–1200	4.18859	–0.15361	14.1	13.5/15.2	18.88/34.64

The change of the Larson–Miller parametric dependence slope in the temperature range of about 700 °C may be due to the dispersed carbonitride V(C,N) particles' coagulation, which have a significant impact on the creep resistance of steels, as well as the ferrite depletion by alloying elements. Carbides enriched with vanadium, found in specimens after testing at temperatures of 700 °C and above, can be attributed to relatively large particles that are no longer crucial for deformation resistance under creep conditions.

This fact is indirectly supported by an abrupt change in the value of the creep stress exponent n for the temperature range of 650–700 °C (Figure 4). A high value of $n > 8$ is observed at test temperatures below 650 °C, which is typical for dispersion-hardened alloys in the "cold" deformation temperature region, when dislocations are not able to redistribute and are forced to move through obstacles in the form of carbides [40]. At 700 °C, the value of the exponent n is 5.35, corresponding to an intermediate state between "warm" deformation (low-temperature dislocation climb controlled by pipe diffusion dominates) and "hot" deformation (high-temperature dislocation climb controlled by lattice diffusion dominates).

The dependence of $\log B(T)$ (Figure 3) also reflects the transition in creep mechanisms from "cold" to "hot" deformation. It is worth noting that if the test duration does not exceed 1 h, the creep parameters can be described with satisfactory accuracy using the Larson–Miller parametric dependence for the temperature range 500–700 °C. However, if the test duration exceeds 20 h, the particular parametric dependence for a temperature range of 700 °C–A_1 is needed. This suggests that the creep mechanism may have changed from "cold" to "warm" and then from "warm" to "hot" deformation during the testing process, as the metal stayed at the test temperature for longer and has undergone microstructure changes.

Obviously, the separation of the Larson–Miller parametric dependence used in this study is quite conditional, as the size of the carbides rises gradually with test temperature and duration increase. Therefore, with more experimental data, we should expect a smooth change rather than an abrupt change in the slope of the parametric dependence.

For a test temperature range of 750–1200 °C, values of the creep stress exponent $n \approx 4.2$–4.9 are observed, which are specific for alloys with solid-solution hardening in the "hot" deformation region. Microstructure and phase transformations in the A_1–A_3 region (Figure 3) are not reflected in the graph of the dependences $\log B(T)$ and $n(T)$, suggesting that the role of carbides in creep deformation resistance at temperatures of 750 °C and above is minimal. In the "hot" deformation region, dislocations can redistribute perpendicular to their sliding planes over long distances due to high-temperature creep controlled by volumetric diffusion. This allows dislocations to bypass obstacles, resulting in low values of creep resistance. The value of the coefficient K in the Monkman–Grant ratio at 750 °C increases approximately twice compared to stable values in the range of 600–700 °C (Figure 4), which indicates significant microstructure changes and the impact reduction of carbides in deformation resistance. This can be interpreted as an increase in the strain rate at the same rupture time.

The abrupt change in creep parameters within the A_1–A_3 range can be explained by the increased creep resistance of austenite phase compared to ferrite at the same temperature. Therefore, with a similar rupture time, the strain rate at 800 °C turned out to be higher than at 850 °C, since the decrease in deformation resistance with temperature increase was compensated by an enlargement in austenite share up to 100%. Similar conclusions were reported in [41], where it was noted that the rupture time of SA508 steel was shorter at a temperature of 750 °C compared to 800 °C.

An important result of this paper is that at temperature range of A_3—1200°C, the creep parameters remain stable and predictable (Figures 3 and 4). So, within this temperature range, the rupture time can be predicted based on the stress and temperature using the Larson–Miller parametric dependence. The exponent n also remains constant, and the increasing trend of the $B = A\exp(-Q/RT)$ parameter within the A_3—1200 °C range (Figure 3) may be related to an increase in temperature, while the value of volumetric diffusion activation energy remains unchanged. This allows us to define a relationship between the minimum strain rate and the applied stress. In fact, the constant value of the coefficient K in the austenitic region (Figure 4) makes it possible to predict the rupture time τ_r based on the minimum strain rate $\dot{\epsilon}_{min}$, even without accurate temperature data.

Figure 7 shows the calculated dependence of the long-term strength limit of 15Kh2NMFAA steel on temperature, obtained on the basis of 1, 10, and 100 h. A noticeable change in the slope of this dependence at a stress level of about 150 MPa (Figure 7) corresponds to the Larson–Miller parameter $P_{LM} = 24.9$, where a break in the linear dependence in Figure 6 also occurs. Obviously, the change in creep characteristics in the range of 600–700 °C should be smooth, as the current microstructure state of the steel depends not only on the temperature but also on the dwell time. An abrupt change in the creep characteristics in the phase transformations' region looks quite justified; however, the deformation nature under creep conditions in the A_1–A_3 range is not entirely clear, and therefore, Figure 7 is shown as dashed lines in this region.

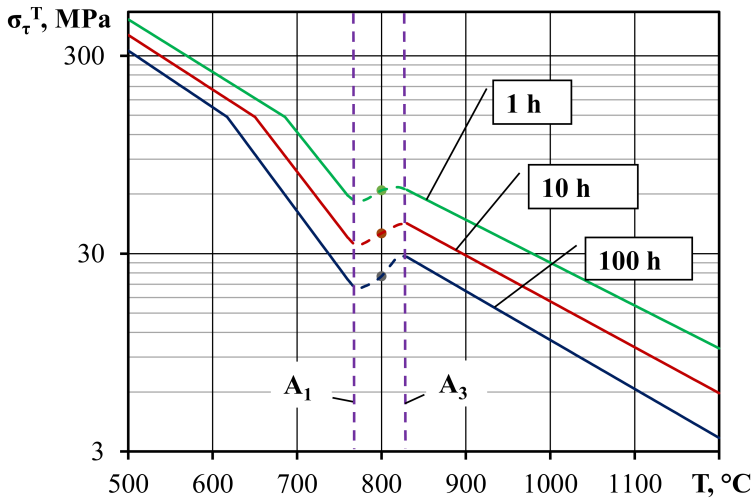

Figure 7. Calculated dependence of the long-term strength of 15Kh2NMFAA steel on temperature.

5. Conclusions

The deformation behavior of 15Kh2NMFAA vessel steel under creep conditions at high temperatures in the range of 500–1200 °C was investigated, and as a result, the following main conclusions were drawn.

It was determined that the transition process from "cold" to "hot" deformation at temperatures of about 700 °C is accompanied by a shift in the trend line of the Larson–Miller parametric dependence, which can be attributed to the coagulation of dispersed carbonitrides of type V(C,N). Although large carbides of different types remained in the metal structure up to 900 °C, with a short testing time, they did not impact significantly the creep process.

It was established that phase transformations within the A_1–A_3 temperature range lead to a break in the Larson–Miller parametric dependence for the steel under study. In such cases, phase transformations do not impact the constants (B, n) of the power law dependence of the strain rate on the applied stress.

It was found that in the austenitic region, the empirical coefficients of the Larson–Miller parametric relation and the coefficient K of the Monkman–Grant ratio, as well as the constants of the power law dependence of the minimum strain rate on the applied stress remain constant for 15Kh2NMFAA steel up to at least 1200 °C. As a result, we obtained a significant practical conclusion, which is that for this steel in the range of 850–1200 °C, we can estimate the time to rupture by the minimum creep rate, even without knowing the value of the actual temperature and its change.

It was found that when dividing the Larson–Miller parametric dependence for 15Kh2NMFAA steel at temperatures around 700 °C, A_1 and A_3 into four sections, the accuracy of rupture time prediction in creep conditions increases by an order of magnitude. Based on the results, the calculated long-term strength limit dependence of 15Kh2NMFAA steel on temperature on the basis of 1, 10, and 100 h was obtained, demonstrating an atypical dependence of creep resistance on temperature in the region of the phase transformations.

Author Contributions: Conceptualization, E.T. and A.M.; Funding acquisition, A.M.; Investigation, E.T., A.M., V.L., A.P., G.S., K.B., D.C. and N.L.; Methodology, E.T. and A.M.; Project administration, E.T.; Experiments, G.S., N.L. and D.C.; Data analysis, A.M., E.T., A.P. and K.B.; Writing—original draft, A.M.; Writing—review and editing, A.M. and E.T. All authors have read and agreed to the published version of the manuscript.

Funding: The research was conducted at the National Research University "Moscow Power Engineering Institute" with funding from the Russian Science Foundation (RSF) under grant No. 23-79-10140, https://rscf.ru/project/23-79-10140/ (accessed on 15 April 2025).

Data Availability Statement: The original contributions presented in this study are included in the article. Further inquiries can be directed to the corresponding author.

Conflicts of Interest: The authors declare no conflicts of interest.

Appendix A

Table A1. Results of tensile creep tests of 15Kh2NMFAA steel

T, °C	Test No.	Stress σ, MPa	Rupture Time τ_r, h	Test Environment	T, °C	Test No.	Stress σ, MPa	Rupture Time τ_r, h	Test Environment
500	1	370	20.0	air	850	29	50	2.1	argon
	2	370	13.6			30	50	2.0	
	3	350	41.0		900	31	48	0.6	argon
	4	350	64.3			32	48	0.5	
600	5	195	46.1	air		33	45	1.0	vacuum
	6	195	40.5			34	44	1.0	argon
	7	260	1.4			35	32	6.5	vacuum
	8	260	1.6			36	27	18.0	
650	9	140	19.3	air		37	25	27.0	
	10	140	17.3			38	22	46.8	
	11	180	2.1		1000	39	25	1.6	vacuum
	12	180	1.6			40	20	5.7	
	13	180	1.4			41	15.5	9.4	
	14	180	2.4			42	13.5	18.9	
	15	200	0.4		1100	43	19	0.6	vacuum
700	16	130	0.8	argon		44	14.3	2.1	
	17	130	0.7			45	12	4.6	
	18	65	21.0			46	10	10.7	
	19	65	23.1			47	9	17.5	
750	20	70	1.1	argon		48	7.7	35.5	
	21	70	0.8		1200	49	10	1.1	vacuum
	22	70	0.8			50	7.6	3.3	
	23	35	21.3			51	7	4.2	
	24	35	20.2			52	6.3	7.2	
800	25	60	0.9	argon		53	5.7	11.6	
	26	60	1.1			54	5.7	11.5	
	27	30	25.4			55	5.1	20.0	
	28	30	21.8			56	4.4	30.8	

References

1. Kymäläinen, O.; Tuomisto, H.; Theofanous, T.G. In-vessel retention of corium at the Loviisa plant. *Nucl. Eng. Des.* **1997**, *169*, 109–130. [CrossRef]
2. Theofanous, T.G.; Maguire, M.; Angelini, S.; Salmassi, T. The first results from the ACOPO experiment. *Nucl. Eng. Des.* **1997**, *169*, 49–57. [CrossRef]
3. Rempe, J.L.; Knudson, D.L.; Condie, K.G.; Suh, K.Y; Cheung F.-B.; Kim, S.-B. Corium retention for high power reactors by an in-vessel core catcher in combination with External Reactor Vessel Cooling. *Nucl. Eng. Des.* **2004**, *230*, 293–309. [CrossRef]
4. Loktionov, V.; Mukhtarov, E.; Lyubashevskaya, I. Features of heat and deformation behavior of a VVER-600 reactor pressure vessel under conditions of inverse stratification of corium pool and worsened external vessel cooling during the severe accident. Part 1. The effect of the inverse melt stratification and in-vessel top cooling of corium pool on the thermal loads acting on VVER-600's reactor pressure vessel during a severe accident. *Nucl. Eng. Des.* **2018**, *326*, 320–332.
5. Loktionov, V.; Mukhtarov, E.; Lyubashevskaya, I. Features of heat and deformation behavior of a VVER-600 reactor pressure vessel under conditions of inverse stratification of corium pool and worsened external vessel cooling during the severe accident. Part 2. Creep deformation and failure of the reactor pressure vessel. *Nucl. Eng. Des.* **2018**, *327*, 161–171.
6. Carénini, L.; Fichot, F.; Seignour, N. Modelling issues related to molten pool behaviour in case of In-Vessel Retention strategy. *Ann. Nucl. Energy* **2018**, *118*, 363–374. [CrossRef]
7. Fichot, F.; Carénini, L.; Sangiorgi, M.; Hermsmeyer, S.; Miassoedov, A.; Bechta, S.; Zdarek, J.; Guenadou, D. Some considerations to improve the methodology to assess In-Vessel Retention strategy for high-power reactors. *Ann. Nucl. Energy* **2018**, *119*, 36–45. [CrossRef]
8. Wang, H.; Villanueva, W. Structural behavior of an ablated reactor pressure vessel wall with external cooling. *Ann. Nucl. Energy* **2022**, *153*, 104446. [CrossRef]
9. Gencheva, R.; Stefanova, A.; Groudev, P.; Chatterjee, B.; Mukhopadhyay, D. Study of invessel melt retention for VVER-1000/v320 reactor. *Nucl. Eng. Des.* **2016**, *298*, 208–217. [CrossRef]
10. Mao, J.; Zhu, J.; Bao, S.; Luo, L.; Gao, Z. Investigation on Structural Behaviors of Reactor Pressure Vessel With the Effects of Critical Heat Flux and Internal Pressure. *Int. J. Press. Vess. Piping* **2016**, *139*, 139–140. [CrossRef]
11. Mao, J.; Zhu, J.W.; Bao, S.; Luo, L.; Gao, Z.L. Creep Deformation and Damage Behavior of Reactor Pressure Vessel under Core Meltdown Scenario. *Nucl. Eng. Des.* **2018**, *327*, 161–171. [CrossRef]
12. Matejovic, P.; Barnak, M.; Bachraty, M.; Vranka, L.; Tuma, Z. VVER-440/V213 long-term containment pressurization during severe accident. *Nucl. Eng. Des.* **2021**, *377*, 111145. [CrossRef]
13. Sarkar, A.; Sunil, S.; Kumawat, B.; Reddy, G.B.; Kapoor, R.; Kumar, H.; Shrivastav, V. High temperature creep behavior of a low alloy Mn-Mo-Ni reactor pressure vessel steel. *J. Nucl. Mater.* **2021**, *557*, 153293. [CrossRef]
14. Lu, C.; Wang, P.; Zheng, S.; Wu, X.; Liu, R.; He, Y.; Yang, J.; Gao, Z.; Tu, S.-T. Creep behavior and life prediction of a reactor pressure vessel steel above phase-transformation temperature via a deformation mechanism-based creep model. *Fatigue Fract. Eng. Mater. Struct.* **2023**, *46*, 3342–3359. [CrossRef]
15. Lu, C.; Wu, X.; He, Y.; Gao, Z.; Liu, R.; Chen, Z.; Zheng, W.; Yang, J. Deformation mechanism-based true-stress creep model for SA508 Gr.3 steel over the temperature range of 450–750 °C. *J. Nucl. Mater.* **2019**, *526*, 151776. [CrossRef]
16. Gao, Z.; Lu, C.; He, Y.; Liu, R.; He, H.; Wang, W.; Zheng, W.; Yang, J. Influence of phase transformation on the creep deformation mechanism of SA508 Gr.3 steel for nuclear reactor pressure vessels. *J. Nucl. Mater.* **2019**, *519*, 292–301. [CrossRef]
17. Xie, L.J.; Ning, D.; Yang, Y.Z. Experimental study on creep characterization and lifetime estimation of RPV material at 723–1023 K. *J. Mater. Eng. Perform.* **2017**, *26*, 644–652. [CrossRef]
18. Kuleshova, E.; Fedotova, S.; Maltsev, D.A.; Potekhin, A. Trends of Structure Degradation of VVER-1000 Reactor Pressure Vessel Steels Determining Their Performance at Lifetimes of over 60 Years. *Phys. At. Nucl.* **2025**, *87*, 1138–1150. [CrossRef]
19. Lobanov, L.; Kostin, V.; Makhnenko, O.; Zukov, V.; Kostenevych, O. Forecasting of Structural Transformations in Heat Affected Zone Steel Of 15KH2NMFA at Anti-Corrosion Cladding. *Probl. At. Sci. Technol.* **2020**, *2*, 89–96. [CrossRef]
20. Blum, W. Mechanisms of creep deformation in steel. In *Creep-Resistant Steels*; Elsevier: Amsterdam, The Netherlands, 2008; pp. 365–402.
21. Kucharova, K.; Sklenicka, V.; Kvapilova, M.; Svoboda, M. Creep and microstructural processes in a low-alloy 2.25%Cr1.6%W steel (ASTM Grade 23). *Mat. Charact.* **2015**, *109*, 1–8. [CrossRef]
22. Sklenička, V.; Kloc, L. Creep in Boiler Materials: Mechanisms, Measurement and Modelling. In *Power Plant Life Management and Performance Improvement*; Woodhead Publishing: Sawston, UK, 2011; pp. 180–221.
23. Whittaker, M.T.; Wilshire, B. Creep and creep fracture of 2.25 Cr–1.6 W steels (Grade 23). *Mater. Sci. Eng. A* **2010**, *527*, 4932–4938. [CrossRef]
24. Radchenko, V.P.; Afanasyeva, E.A.; Saushkin, M.N. Prediction of creep and long-term strength of material by sample-leader under ductile fracture conditions. *Appl. Mech. Tech. Phys.* **2023**, *64*, 199–209. (In Russian) [CrossRef]

25. Claesson, E.; Magnusson, H.; Kohlbrecher, J.; Thuvander, M.; Lindberg, F.; Andersson, M.; Hedström, P. Carbide Precipitation during Processing of Two Low-Alloyed Martensitic Tool Steels with 0.11 and 0.17 V/Mo Ratios Studied by Neutron Scattering, Electron Microscopy and Atom Probe. *Metals* **2022**, *12*, 5, 758. [CrossRef]
26. Sklenička, V.; Kuchařová, K.; Dvorak, J.; Kvapilová, M.; Král, P. Creep Damage Tolerance Factor λ of Selected Creep-Resistant Steels. *Key Eng. Mater.* **2017**, *754*, 47–50. [CrossRef]
27. Kvapilová, M.; Ohanková, M.; Král, P.; Dvořák, J.; Kuchařová, K.; Čmaka, L.J.; Sklenička, V. Characterization of creep properties and the microstructure of a service-exposed low alloy CrMoV steel steam pipe. *Mater. Sci. Eng. A* **2022**, *853*, 143684. [CrossRef]
28. Kloc, L. Creep of ex-service 0.5 CrMoV steel at low strain rates. *Mater. Sci. Eng. A* **2009**, *510*, 70–73. [CrossRef]
29. Shigeyama, H.; Takahashi, Y.; Siefert, J.; Parker, J. Creep-Fatigue Life Evaluation for Grade 91 Steels with Various Origins and Service Histories. *Metals* **2024**, *14*, 148. [CrossRef]
30. Saxena, A. A Phenomenological Model for Creep and Creep-Fatigue Crack Growth Rate Behavior in Ferritic Steels. *Metals* **2023**, *13*, 1749. [CrossRef]
31. Zheng, Q.; Zhong, W.; Bai, B.; Yang, W.; Wang, Z.; Huang, C. Research on the Fracture Behavior and Microstructure of T91 Steel at Ultrahigh Creep Temperatures. *Metals* **2022**, *12*, 2054. [CrossRef]
32. Dudova, N. 9–12% Cr Heat-Resistant Martensitic Steels with Increased Boron and Decreased Nitrogen Contents. *Metals* **2022**, *12*, 1119. [CrossRef]
33. Di Pompeo, V.; Santoni, A.; Santecchia, E.; Spigarelli, S. On the Short-Term Creep Response at 482 °C (900 °F) of the 17–4PH Steel Produced by Bound Metal Deposition. *Metals* **2022**, *12*, 477. [CrossRef]
34. Kassner, M.E. New Developments in Understanding Harper–Dorn, Five-Power Law Creep and Power-Law Breakdown. *Metals* **2020**, *10*, 1284. [CrossRef]
35. Loktionov, V.; Lyubashevskaya, I.; Terentyev, E. The regularities of creep deformation and failure of the VVER's pressure vessel steel 15Kh2NMFA-A in air and argon at temperature range 500–900 °C. *Nucl. Mater. Energy* **2021**, *28*, 101019. [CrossRef]
36. Loktionov, V.; Lyubashevskaya, I.; Terentyev, E. Regularities of the creep deformation and failure of 15Kh2NMFA-A steel within the temperature range of 900–1200 °C. *Int. J. Press. Vess. Piping* **2022**, *199*, 104745. [CrossRef]
37. Terentyev, E.V.; Marchenkov, A.Y.; Loktionov, V.D.; Lyubashevskaya, I.V.; Chuprin, D.V.; Borodavkina, K.T.; Sviridov, G.B. Investigation of Creep Characteristics of Vessel Steel 15Kh2NMFA-A of WWER-type Reactor at Temperatures 500–1200 °C. *Fact. Lab. Mater. Diagn.* **2024**, *90*, 56–66. (In Russian) [CrossRef]
38. Loktionov, V.; Lyubashevskaya, I.; Sosnin, O.; Terentyev, E. Short-term strength properties and features of high-temperature deformation of VVER reactor pressure vessel steel 15Kh2NMFA-A within the temperature range 20–1200 °C. *Nucl. Eng. Des.* **2019**, *352*, 110188. [CrossRef]
39. Dudko, V.; Yuzbekova, D.; Gaidar, S.; Vetrova, S.; Kaibyshev R. Tempering behavior of novel low-alloy high-strength steel. *Metals* **2022**, *12*, 2177. [CrossRef]
40. Kaybyshev, R.O.; Skorobogatykh, V.N.; Shchenkova, I.A. New martensitic steels for fossil power plant: Creep resistance. *Phys. Met. Metallogr.* **2010**, *109*, 186–200. [CrossRef]
41. Baker, T.N. Processes, microstructure and properties of vanadium microalloyed steels. *Mater. Sci. Technol.* **2009**, *25*, 1083–1107. [CrossRef]